Experimental and numerical analysis on the structural fire behaviour of three-cell hollowed concrete masonry walls

Rafael G. Oliveira[1]; João Paulo C. Rodrigues[1,*]; João Miguel Pereira[2]; Paulo B. Lourenço[2]; Ruben R. Lopes[1]

[1]Civil Engineering Department. Coimbra University. Portugal

[2]ISISE – Institute for Sustainability and Innovation on Structural Engineering. Civil Engineering Department. Minho University. Portugal

[*]corresponding author: jpaulocr@dec.uc.pt

Abstract

Masonry is one of the oldest and most traditional materials in building construction. Nevertheless, the knowledge on the structural fire behaviour of masonry elements is not yet well consolidated. The literature on the load-bearing capacity of masonry walls in case of fire showed an enhanced performance of these elements, however the lack of normative documents, characterization of material properties at high temperatures and experimental results, for calibrating and validating the numerical models, indicates the need of further research. A research study on the structural fire behaviour of three-cell hollowed concrete masonry walls subjected to fire is presented based on results of experimental and numerical studies. First, several loadbearing capacity tests at high temperatures and fire resistance tests on the walls, were carried out in order to assess their behaviour, critical times, failure modes and temperature distribution. The specimens were built with three cell concrete blocks and M10 mortar and were then subjected to an in-plane serviceability load during test. The temperatures, loads and displacements were measured. Second, finite element models were developed and validated with the experimental results. The experimental and numerical results were also compared with the ones given by EN1996-1-2 provisions.

Keywords: fire, resistance, concrete masonry wall, experimental and numerical analysis

Notation:

f_{ak} - characteristic value of the compressive strength normal to bed joints at ambient temperature;

f_d - design value of the compressive strength normal to bed joints at ambient temperature;

$N_{rd\,fi}$ - design value of the in-plane resistance of a masonry wall at high temperatures;

h - height of the wall;

d_C/d_t - rate of vertical contraction;

C - vertical contraction;

K_c - ratio of the distances between the hydrostatic axis and, respectively, the compression meridian and the tension meridian in the deviatory plane;

ψ - dilation angle;

ε – eccentricity;

μ - viscosity parameter.

1. INTRODUCTION

Concrete masonry has been used worldwide all over the centuries in loadbearing and partition walls. To provide safety of such structures in fire situation, requirements related to insulation, integrity and stability must be attended. In Europe, the EN1996-1-2 standard (Eurocode 6, part 1-2) [1] states that masonry walls must meet one or more of the following requirements when exposed to fire: **I** for temperature insulation, **E** for integrity avoiding smoke and hot gases passing through the wall, **R** for loadbearing capacity and stability and **M** for mechanical impact resistance when required.

In fire situation, masonry walls are usually subjected to heating on one face, which leads to a thermal gradient through their thickness. In restrained walls the differential thermal elongation may result in thermal bowing, a complex phenomenon that depends on the composite material properties which are temperature dependent [2]. The material properties degradation caused by the high temperatures, associated with the thermal strains, may lead to the structural collapse of the wall [3]. Therefore, the structural stability of masonry walls is required during fire to prevent collapse and fire spread, mitigate local structural collapse and guarantee the safe evacuation of the building occupants [4].

The research presented in this paper includes an experimental and numerical study on the structural behaviour of a type of concrete masonry wall subjected to fire. The tested walls were built with three-cell calcareous aggregate concrete blocks and M10 mortar. In the fire resistance tests, the walls were subjected to an in-plane load and heated according to the ISO 834 standard fire curve [5-6]. The temperatures were measured in the gas inside the furnace and in the non-exposed face of the wall. In-plane and out-of-plane displacements were measured in the specimens. The experimental results were used to calibrate numerical models developed with Abaqus software and compared with the EN1996-1-2 predictions [1].

The numerical models were calibrated with the experimental results from ambient temperature [7] and high temperature tests presented in this paper. The experimental and numerical results are in good agreement and allow to better understand fire performance of masonry walls. Finally, the obtained results were compared with the ones from the European and Australian code provisions.

The present study tries to fulfil a gap in the literature, providing experimental results for characterizing the behaviour of concrete masonry walls composed of three cells hollowed blocks in case of fire. The proposed finite element model was able to represent the masonry behaviour with reasonable accuracy. EN1996-1-2 [1], for concrete masonry block walls subjected to fire is generalist and does not have specific values for concrete block walls of one or two cells. The Eurocode's simplified calculation and tabular methods overestimate, in general, the fire resistance of this type of walls.

1.1. Experimental research on masonry walls subjected to fire

The previous experimental researches on masonry walls subjected to fire are discussed in this section. Byrne [8], in 1979, was maybe the first working in the area. He has conducted a series loadbearing capacity tests at high temperatures in clay brick masonry walls. The influence of the slenderness and load level on the thermomechanical behaviour was studied. The author defined the basic theories and influences of the thermal diffusivity, thermal elongation, thickness and height of the walls and load level, in the behaviour of the walls in case of fire.

Lawrence and Gnanakrishnan [9], in 1987, presented a state of the art on the structural behaviour of masonry walls subjected to fire, evaluating the existing design concepts and standards and defining a roadmap approach for future researches.

Shields et al. [10], in 1988, studied the thermal bowing effects and the influence of the differential heating on the behaviour of calcium silicate masonry walls. The authors explained why the thermal bowing has influence on the structural behaviour of the wall in case of fire.

Nahhas et al. [11], in 2007, investigated the thermo-mechanical behaviour of hollow brick masonry walls in case of fire. The experimental results studied the phase-change effects, associated to plateaus in the temperature and displacement curves at around the 100 ºC corresponding to the free water evaporation. The authors used an enthalpy methodology to incorporate the energy absorption by liquid water evaporation under a form of equivalent specific heat around the temperature of ebullition.

Nguyen and Meftah [12], in 2012, performed load-bearing capacity tests on clay hollow-brick walls subjected to fire. The authors studied the effects of parasitic bending moments generated at high temperatures in the walls. They have also highlighted that in numerical modelling a three-dimensional analysis is required for investigating the non-linear behaviour of masonry walls in fire situation.

Andreini et al. [13], in 2015 determined the mechanical properties at high temperatures of bricks and mortars. The results of this research and the ones of EN1991-1-2 [6] and EN 1996-1-2 [1] for the material properties, were used in the numerical simulations presented in this article.

With regard to the mechanical properties at ambient temperature of the bricks used in the present research, the results of Haach [7], presented in 2007, were used. The author presented results of compressive tests in the direction normal and parallel to the bed joints, shear and flexural tests. This study was used, in the present research, on the calculation of the loads applied to the walls in the experimental tests and calibration of the numerical models.

1.2. Numerical research on masonry walls subjected to fire

O'Meagher and Bennetts [14], in 1999, used a computer-based method for analysing concrete masonry walls in fire, taking into account the material and geometrical non-linearity. The influence of the effective height and thermal restraining on the stability and loadbearing capacity of the walls were investigated.

Nadjai et al. [3], in 2003, developed a thermo-structural finite element model (MasSET) for extruded clay brick walls subjected to fire. A parametric study was carried out to investigate the effects of the slenderness, load eccentricity and boundary conditions on the masonry walls subjected to fire [4]. However, the developed numerical models were not able to simulate the behaviour of masonry blocks with cavities.

Nguyen and Meftah [15], in 2014, presented a numerical model to investigate the behaviour of fired-clay masonry walls subjected to fire. A three-dimensional numerical simulation was conducted with particular attention to the spalling of the hollow bricks.

Kumar and Kodur [16], in 2017, proposed a model to predict the fire response of loadbearing reinforced concrete walls. The high thermal inertia of the concrete masonry walls, without cavities, led to high thermal gradients. The authors found that the structural response of the walls was first characterized by a rapid increasing of the out-of-plane displacements resulting from the thermal gradient through the wall's thickness. In a second stage a shift in the position of the neutral axis caused by the degradation of the material properties at high temperatures, occurred. The last stage was characterised by a reverse of the thermal bowing, where the effects of the neutral axis shift overlap the thermal elongation of the wall. In these works, [15-16] were also numerically tested hollow brick walls at high temperatures.

2. EXPERIMENTAL TESTS

The experimental program carried out comprised four fire resistance tests and two compressive tests after 90 min of fire exposure in half scale loadbearing concrete masonry walls. The specimens were built with

three-cell concrete blocks that are common in building construction around the world [7]. The walls were subjected to a serviceability in-plane load and, subsequently, heated according to the ISO 834 standard fire curve [5 and 6].

2.1. Masonry units

Three-cell hollow concrete masonry units were used in the fabrication of the specimens [7]. Half-scale units were used (Fig. 1) and their dimensions are presented in Table 1. These units fit in group 2 of EN 1996-1-1 [17], due to the size, orientation and dimensions of the holes. The masonry block units were made with dense aggregate concrete.

2.2. Experimental tests at ambient temperature

The mechanical proprieties at ambient temperature of the masonry was determined by Haach [7]. The author tested the units, mortar and masonry wall specimens under different conditions, namely three masonry specimens under compression normal to bed joints and initial shear strength according to EN1052-1 and EN 1052-3 [18 and 19], respectively. The geometry of the specimens was defined according to this European standard and is presented in Fig. 2a. Four LVDTs were used to measure the in-plane displacements of the wall and two used to measure the out-of-plane displacements (Fig. 2b). The Young's modulus of the masonry was determined based on the strain-stress curve.

Haach [7] also performed flexural tests on masonry walls according to EN1052-2 [20] (Fig. 3). Three specimens were built with two units in length and seven courses in height with 8 mm joints (Fig. 3a). Three LVDTs were used to measure the in-plane displacements (Fig. 3b). The flexural stiffness of the masonry walls could be calculated based on the moment versus curvature diagram. The curvature is defined based on the readings of the LVDTs installed at the bottom of the specimen.

The experimental results provided by Haach [7] were also used for determining the mechanical properties of the homogenised material to numerically model the masonry (see section 4.1), namely the: Young´s modulus, Poisson's ratio, compressive and tensile strengths.

2.3. Experimental tests at high temperatures

The specimens for the fire resistance tests and loadbearing capacity tests at high temperatures had seven block units in length (1.40 m) and ten in height (1.00 m) (Fig. 4). The wall's dimensions were decided according to the limitations of the load application system and reaction frames existing in the laboratory. Bigger walls would need the application of higher loads. On the other hand, these dimensions were also limited by the front opening of the electric furnace used to heat the wall's face.

The horizontal joints were made of M10 mortar and had 7 mm thickness, and were built according to EN 998-2 [21]. The test instrumentation was in agreement with the standard EN 1365-1 [22]. Eleven thermocouples were installed at the non-exposed face of the wall. Three LVDTs were used to measure the out-of-plane displacements at the centre of the sample. Three LVDTs were also used to measure the in-plane displacements at the top of the wall in the load distribution beam. Full details of the experimental tests can be found in [23 and 24].

2.3.1. Test set-up

The experimental setup is composed by a reaction frame made with HEB 300 steel profiles (**Erro! A origem da referência não foi encontrada.**Figs 5 and 6).

The load was applied by a 1 MN hydraulic jack controlled by a Walter + Bai NSPA 700 / DIG 2000 servo-controlled central unit. A TML TDS-530 data logger was used to register the experimental data during the tests. The heating curve was applied using an electric furnace capable to reach the ISO 834 fire curve [5 and 6] with reasonable accuracy. The internal dimensions of the furnace were 1.50x1.00x0.75 m. A TML load cell (500kN) was used to measure the load applied to the walls during the tests.

2.3.2. Test procedure

The experimental program comprised three different types of loading with two equal specimens for each loading level. A total of six walls were tested.

In the fire resistance tests 1 and 2, the specimens were first subjected to 30% of f_{ak}, applied at a rate of 0.5 kN/s, and then heated according to the ISO 834 standard fire curve [5 and 6] up to rupture. In the fire resistance tests 3 and 4, the specimens have been tested in a similar way to the previous, but with 46% of f_{ak}. In the loadbearing capacity tests at high temperatures 5 and 6, the specimens were first subjected to 30% of f_{ak}, applied at a rate of 0.5 kN/s, and then heated up to 90 min of the ISO 834 fire curve [5 and 6], after this the load was increased at a constant rate of 0.05 kN/s until rupture of the specimen. The in-plane loads applied to the specimens are summarized in Table 2.

3. EXPERIMENTAL RESULTS

3.1. Temperatures

The temperatures at the non-exposed face are used to determine the insulation capacity of the wall (**I**). As an example, the results for test 6 are presented in Figure 7. The gas temperatures inside the furnace followed approximately the ISO 834 standard fire curve. There is a small delay in the temperature rise, in the

beginning of the test, due to the thermal inertia of the electrical furnace and high capacitance of the materials of the wall.

Concerning the temperature in the wall, at the beginning of fire exposure (about 15 min.), there was no increase in the non-exposed face due to the thermal inertia. The temperatures started to increase at an approximate constant rate, up to 100ºC. At this stage, the free water of the constitutive materials of the wall (blocks and mortar) started to evaporate and a plateau in the temperatures was observed. This plateau lasted for 10 to 30 minutes, depending of the zone of the wall. The thermocouple installed at the top of the wall (a1) presented a plateau that lasted for around 30 minutes, however the thermocouples installed at middle-height of the wall (d1 and m3) presented a plateau that lasted for only 10 minutes. This difference was possibly due to the steam flow through the vertical holes of the blocks, which led to steam accumulation at the top of the wall, cooling this area. After the free water evaporation, the temperatures started to rise again. During the entire test, it was possible to observe a clear thermal gap through the thickness of the wall that remained approximately constant after the evaporation of the free water.

3.2. Displacements

The in-plane displacements of the specimen of test 6, as an example, are presented in Figure 8. During the first 15 minutes of test, there was no increase in the in-plane displacements. After this point, there was an increase of the displacements due to the thermal elongation of the wall, up to 60 minutes. From 60 to 90 minutes of fire exposure, there is an attenuation in the increasing of the displacements. After 90 minutes of fire exposure, associated to the increasing of the in-plane load and the degradation of the material's properties due to the high temperatures, a decreasing of the in-plane displacements was observed, meaning that the wall collapsed.

The out-of-plane displacements of the specimen of test 6 are presented in Figure 9. During the first 5 minutes of test, there was no increasing in the displacements. After this point, there was an increasing of the displacements towards the fire due to the thermal gradient through the thickness of the wall, up to 60 minutes. From 60 to 90 minutes of fire exposure, it was possible to identify a plateau in the out-of-plane displacements. After this point, a reverse bowing was observed and the out-of-plane displacements started to decrease until the end of the test.

The in-plane and out-of-plane displacements of the tested specimens are presented in Figures 10 and 11, respectively. Based on these results it is possible to identify a significant scattering in the results, typical of masonry structures. The reverse thermal bowing was identified for specimens 2, 3, 5 and 6, however, it was not observed in the specimens of tests 1 and 4.

3.3. Visual assessment

Vertical cracks appeared at around 30 minutes after the beginning of the test, with a clear condensation of the water vapour that emerges through these cracks in the external face of the wall (Fig. 12a). The vertical cracks started near the centre of the blocks being coincident with their central cells and head joints. Horizontal cracks were found, predominately, at the block-mortar interfaces and diagonal cracks started at the corner of the specimen and propagated to the centre. Spalling was also visible in the exposed face after the tests (Fig. 12b).

Vertical cracks (Fig. 12c) were found at mid-thickness of the walls. These cracks are possibly caused by parasitic bending moments similar to the ones found in the works of Nguyen and Meftah [12]. Moreover, there were imperfections at this region of the blocks, due to the fabrication process, that could have further induced crack occurrence at this point.

Specimens 3 to 6 presented a brittle failure, without warning signs such as huge displacements or sudden loss of stiffness. The sequence of collapse is presented in Figure 13 for specimen of test 6, as an example. It can be seen that the failure was initiated at the bottom of the wall, with total loss of material and strength.

4. NUMERICAL ANALYSIS

As presented by Lourenço et al [25], numerical modelling of masonry structures may adopt different approaches. Pereira et al [26] summarized these techniques: (a) detailed micro-modelling: where block units and mortar are represented by continuous elements and the unit-mortar interface is represented by discontinuous elements (or interaction between elements); (b) simplified micro-modelling, where expanded units are represented by continuous elements and the behaviour of joints and mortar-joints interfaces is lumped in discontinuous elements; and (c) macro-modelling, where a homogeneous continuous material is used to represent the behaviour of the block units, mortar and interfaces.

The numerical analyses presented in this work were performed using the finite element software Abaqus [27]. The geometry of the model was based in the description provided at section 2. A macro-modelling strategy was adopted, therefore, the masonry walls were considered homogeneous and isotropic. Consequently, there is no contact condition between the brick and the mortar, as only one material represents the wall. This technique has been successfully used by other authors to model masonry structures both at ambient and high temperatures [2, 3, 11, 15 and 26]. The Abaqus Explicit solver was used in the numerical simulations with good results and it has been done by several other authors [26, 28 and 29].

4.1. Analysis procedure

The developed finite element model comprised three types of analysis that were performed separately: elastic buckling, heat transfer and nonlinear mechanical analysis.

An elastic buckling analysis is performed to assess the buckling modes of the wall. To carry-out this analysis, the boundary conditions, mechanical properties and mechanical loads were introduced in the numerical model. The suitable buckling modes obtained were used in the definition of the initial geometrical imperfections of the mechanical testing models.

A heat transfer analysis was used to determine the temperature distribution in the wall. The model was fed with the specific heat, thermal conductivity and density of the materials, taken as temperature-dependent (see 4.3). The initial temperature and the gas temperature of the furnace were also inputted. Moreover, the heat transfer mechanisms of convection and radiation and cavity radiation were defined. The emissivity of the materials and convection factors were taken as non-temperature-dependent, as stated in EN 1992-1-2 [6].

The heat transfer between the faces of the wall was modelled taking into account three modes: convection, conduction and radiation. At the exposed face, the radiation and convection effects of the fire were also modelled. Conduction in the solid parts and radiation inside the cavities of the blocks were also considered. At the non-exposed face, the radiation and convection at ambient temperature were taken into account. Figure 14 summarises the heat transfer process through a hollow block.

The exposed wall's surface was assumed to be all, in each instant, at the same temperature. This was confirmed by thermocouples installed in the specimens in the experimental tests. Therefore, the temperatures considered vary only through the thickness of the wall. The material properties were considered as temperature-dependent. The radiation at the exposed and non-exposed face was represented as a surface radiation, the radiation at the cavities was represented as cavity radiation and the convection was represented as a surface film condition. The convection coefficient was taken as 25 W/m^2 $^\circ$C and the emissivity of the concrete masonry was taken as 0.70, as indicated in EN 1992-1-2 [6]. The gas temperatures inside the furnace during the tests were used to perform the heat transfer analysis. Due to the thermal insulation material used in the experimental system, adiabatic surfaces were considered between the wall and the reaction slab, the lateral constraining walls and the loading beam. Consequently, all heat losses took place by the non-exposed face.

Finally, a mechanical analysis up to failure was performed to simulate the behaviour of the concrete hollow masonry walls in fire. To carry-out this analysis, the mechanical properties of the material (see 4.3), initial imperfections, mechanical loads, temperature fields and boundary conditions were defined.

4.2. Finite element mesh, boundary, loading and contact conditions

The masonry walls were discretized with 8-node solid elements. The final mesh was generated automatically by Abaqus software and was rather refined. The influence of the finite element size on the behaviour of masonry walls was evaluated and it was found that the 8mm x 8mm x 8 mm elements would lead to adequate simulation results (Fig. 15).

For the heat transfer analysis, the 8-node linear heat transfer elements (DC3D8) were used. The C3D8R elements were used for the mechanical analysis. This type of element is a three dimensional continuum hexahedral brick element with reduced integration (R), hourglass control and linear interpolation, with three degrees of freedom per node, (translations in directions X, Y and Z).

Nguyen and Meftah [12] emphasized that a two-dimensional (in-plane) modelling approach, although usually adopted for design of masonry structures, may preclude some critical failure mechanisms that affect the occurrence of spalling, and they recommend the use of a three-dimensional modelling of such structures. Therefore, a three-dimensional numerical model was used to increase the accuracy of the numerical model.

As observed in the experimental setup, the masonry support and the loading were applied on rigid elements attached to the beams aiming to distribute the concentrated load on them. A hard contact was assumed between the masonry and the rigid elements, in other words a perfect contact condition was used, consequently, there is no overclosure or clearance between these surfaces. The CDP (Concrete Damage Plasticity) model assumes that failure under compressive crushing and tensile cracking is defined by damage plasticity. The constitutive model used the concept of isotropic damage evolution to represent the inelastic behaviour of the material.

4.3. Material properties

Thermal fields during the test were determined based on heat transfer analysis. The material properties of the concrete masonry were determined based on the values presented at EN 1992-1-2 [30] and EN 1996-1-2 [6]. The thermal conductivity curve for limestone concrete presented at the French National Eurocode Annex of EN 1992-1-2 was used. The density, specific heat and thermal elongation were taken as stated by EN 1992-1-2 [6]. Figure 16 summarizes the thermal properties used.

The CDP model is a modification of the Drucker-Prager model [31, 32], where the shape of the failure surface, in the deviatoric plane, does not need to be a circle and it is defined by the parameter Kc that can be defined as a ratio of the distances between the hydrostatic axis and, respectively, the compression meridian and the tension meridian in the deviatoric plane. Kc was taken as 0.667 [26]. The dilation angle (ψ) was taken as 20º, the eccentricity (ε) as 0.10, the ratio of the initial equibiaxial compressive yield stress to initial uniaxial compressive stress as 1.16 and the viscosity parameter as 0.02. These parameters were taken as non-temperature-dependant. The compressive and tensile strengths of the masonry were taken as temperature dependant.

The homogenised mechanical properties were taken from the experimental tests performed by Haach [7], as shown in section 2.2. The Young's modulus was considered as 22800 MPa, the compressive strength as 10.5 MPa and the tensile strength as 0.8 MPa. The coefficients of reduction of the mechanical properties considered were the ones proposed at EN 1992-1-2 [30] and EN 1996-1-2 [6].

5. VALIDATION OF THE NUMERICAL MODEL

5.1. Temperatures

Figure 17 shows a comparison of the temperature curves of the non-exposed face of the masonry between the experimental tests and the finite element analysis (FEA), used for validation of the model. The curves from FEA fit well the experimental range of temperatures. This agreement between the experimental and numerical results provides a strong validity of the developed finite element model. The experimental values measured by the thermocouples (Exp.TP.MX), the predicted numerical values of the hot face (Num.HF) and cold face (Num.CF) and the temperatures measured in the furnace (Furnace) and ISO 834 standard fire curve (ISO) are presented in Figure 17.

The developed model reproduced all stages of the heating described at Section 3.1 with good agreement: the plateau of temperatures at the non-exposed face at the beginning of the tests, the plateau of temperatures at around 100ºC due to the evaporation of the free water of the masonry elements and the heating stages. The experimental values presented some scatter in the temperatures between the locations of the thermocouples that were not reproduced by the numerical model, as the finite element model is not able to reproduce the steam flow inside the cavities of the blocks nor the migration of interstitial water. However, these small differences between the numerical and experimental results may result also from differences in the moisture level of the masonry, air convection inside the furnace and ambient conditions during the tests. As concluded by Nguyen and Meftah [12], it was observed that the heat transfer within the masonry walls

is mainly radiative and convective, as the cavity radiation (the radiation that takes place inside the voids of the blocks) plays an important role on the heat flux during the thermal analysis.

Figure 16d presents the thermal elongation of calcareous concrete versus temperature, according to EN 1992-1-2 [30]. After 800ºC, the material started to expand with the temperature. The furnace reached 800ºC at 60 minutes, approximately the same time when the in-plane displacements rate decreased and the out-of-plane displacements reached a plateau. The constant thermal elongation after 800ºC led to a decrease on the rate of the in-plane thermal strains of the wall, which control the out-of-plane displacements and the thermal bowing.

5.2. Stress, strain and displacements

The validation of the model for these parameters was made first with a comparison of the experimental and numerical results at ambient temperature and after at high temperatures. The validation in terms of ambient temperature was performed comparing the stress-strain curves for uniaxial compression and moment-curvature curves for four-point bending (Fig. 18Erro! A origem da referência não foi encontrada.), based on the experimental results of Haach [7]. Figure 18a shows the strain-stress relation obtained experimentally and numerically at ambient temperature, under uniaxial compression perpendicular to the bed joints. Figure 18b shows a similar comparison but for the moment – curvature applied to the wall. In both cases, a good correlation between the curves was found.

Figures 19 and 20 show a comparison of the numerical with the experimental in-plane and out-of-plane displacements in function of the time, respectively, for fire test 1. The in-plane displacements started to grow from the beginning of the test due to the thermal elongation of the wall. During the test, the effects of the thermal elongation were more important than the reduction of the stiffness of the wall, as positive displacements were found during the whole test. The numerical results were in good agreement with the experimental ones. The out-of-plane displacements started to grow after 45 minutes of fire exposure. Thermal bowing was not observed in this fire test 1.

These results show that the numerical models were capable to simulate the behaviour of the concrete masonry walls subjected to fire. Nevertheless, the masonry is a highly heterogeneous materials and some scattering in the results are expected.

As shown in Figure 19, the numerical in-plane displacements are in good agreement with the experimental ones. The in-plane displacements start to increase since the beginning of the fire exposure, due to the thermal elongation of the wall. Positive in-plane displacements were obtained during the test until the rupture of the specimen.

As shown in Figure 20, there is a plateau in the out-of-plane displacements at the beginning of the test, that lasts up to 60 minutes. After this point, the thermal bowing of the wall is observed. The numerical model was able to represent this phenomenon. However, the lack of thermal and mechanical properties of the materials (blocks and mortar) at high temperatures led to a medium agreement between the numerical and experimental results.

5.3. Analysis and discussion

As observed in the experimental results, masonry is a highly heterogeneous material. Some scatter was found in the results, including the in-plane and out-of-plane displacements, temperatures, critical times and loads, as presented in sections 3.1 and 3.2. Nevertheless, the heat transfer analysis presents good results with the experimental tests. As concluded by Nguyen and Meftah [12], it was observed that the heat transfer within masonry walls is mainly radiative and convective, as presented in section 5.1. It is stressed that the moisture content of the masonry has a great influence on the specific heat of the homogenised material, mostly for temperatures between 100ºC and 115ºC, which leads to a significant impact on the duration of the temperatures plateau at around 100ºC corresponding to the free water evaporation, as stated by Nahhas et al. [11].

The sequential coupled analysis led to a reduction on the required computation resources to perform the numerical calibration, when compared to the coupled thermal-structural analysis. As the same heat transfer analysis may be used to study different conditions with the same geometry, such as load levels, eccentricities and so on.

The CDP model is suitable to represent the behaviour of concrete masonry in fire situations However, there is lack of experimental results to feed the numerical models. Compressive tests and flexural tests performed at different temperatures, from ambient temperature up to 700ºC or more, would generate the required data for modelling and increase the quality of the results.

The thermal characterization of such materials, including thermal elongation, thermal conductivity, specific heat and emissivity, would generate a strong and reliable data base that may be used to analyse and design concrete masonry structures in fire situation.

6. CRITICAL TIMES AND COMPARISON WITH THE CODE PROVISIONS

6.1. Performance criteria

The standard EN 1363-1:1999 [33] states the failure criteria in fire resistance tests are the following:

- **Loadbearing capacity (R)**

The loadbearing capacity is the time in minutes that the specimen continues to maintain its ability to support the load during the test. For vertical loaded elements the limitations are:

    a) limiting the vertical contraction (negative elongation): $C = h / 100$;

    b) limitation the rate of vertical contraction: $d_C/d_t = 3 h / 100$ mm/min;

Where h is the initial height of the wall, in millimetres.

- **Integrity (E)**

The integrity performance is the time in minutes that the specimen continues to maintain its compartmentation function during the test without either:

    a) causing the ignition of a cotton pad;

    b) permitting the penetration of a gap gauge;

    c) resulting in sustained flaming.

- **Insulation (I)**

The insulation performance is the time in minutes that the specimen continues to maintain its compartmentation function during the test without developing temperatures on its unexposed surface which either:

    a) average temperature: increase the average temperature above the initial average temperature by more than 140 ºC;

    b) maximum temperature: increase at any location above the initial average temperature by more than 180ºC.

6.2. Critical times

The critical time (failure time), ultimate loads and maximum out-of-plane displacements obtained in the experimental research are presented in Table 3. The insulation capacity (**I**) presented an average value of 71 minutes for the maximum temperature and an average value of 76 minutes for the average temperature. The loadbearing capacity (**R**) presented an average value of 133 minutes for the load level of 70% f_d and an average value of 61 minutes for the load level of 108% f_d. For specimens 5 and 6, where the initial load level of 70% f_d was increased after 90 minutes of fire exposure, the average failure time was 120 minutes. As highlighted by different authors [10,11,12 and 14] the load level has a significant influence on the fire resistance of masonry structures.

The comparison of the experimental with the numerical results are presented in Table 4. The insulation criteria present similar results for both cases. The loadbearing capacity predicted in the numerical simulations presents also good agreement with the experimental results.

6.3. Comparison with the tabulated data of the European and Australian codes

In this section, the experimental results are compared with the tabulated data of the fire resistance of masonry walls presented in Annex B of EN 1996-1-2 [1]. Table 5 presents the minimum wall thickness indicated in tables N.B:3.1 and N.B.3.2 of EN 1996-1-2 [1] for the EI and REI criteria, respectively. The critical times presented in Table 3 indicates that the failure by insulating criteria (**I**) is reached between 65 and 82 minutes. The failure due to structural collapse (**R**) is reached between 133 and 134 minutes for specimens 1 and 2, between 40 and 83 minutes for specimens 3 and 4, and between 106 and 134 minutes for specimens 5 and 6. Based on the experimental results, concrete masonry walls with dense aggregates and composed by group 2 concrete block units with 100 mm of thickness, are not able to fulfil the EI90, EI120 and EI180 fire class requirements. Moreover, one of the studied walls was not able to fulfil the REI120 requirements for the load level $\alpha \leq 1.0$. The load level α is defined by the ratio of the applied design load in the wall to its design resistance. Therefore, it seems that the values indicated in tables N.B:3.1 and N.B.3.2 of EN 1996-1-2 are unsafe for the analysed walls for both (**EI**) and (**REI**) fire resistance classes. Additionally, there is an inconsistency in the values presented in table N.B.3.1. The minimum range of thickness to fulfil the EI90 requirements (from 70 to 90 mm) is smaller than the required thickness to fulfil the EI60 requirements (from 70 to 100 mm).

The Australian Code AS 3700:2018 - Masonry Structures [34] also presents unsafe values in the tabulated data. According to table 6.3 of that standard, concrete masonry with density higher than 1800 kg/m^3 and 100 mm thickness, should have at least 90 minutes for the insulation criterion (I). In the experimental tests, this criterion failed for a time between 65 and 82 minutes of fire exposure, that is much lower than the value prescribed in this standard. Regarding the structural adequacy, table 6.1 states that concrete masonries, with slenderness ratio smaller than 15.0, should have a fire resistance of 240 minutes. However, the experimental tests, for a wall with a slenderness ratio of 7.5, showed that this fire resistance will be never reached.

6.4. Comparison with the Eurocode simplified calculation method

The simplified calculation method presented in Annex C of EN 1996-1-2 [1] is used to determine the temperature profile of the cross-section, the ineffective and the residual cross section, and then to calculate the loadbearing capacity at the ultimate limit state with the residual cross section.

Table 6 presents the N_{rdfi} calculated for R30 to R240, comparing the predicted values against the experimental results (Table 3). It is possible to conclude that the simplified calculation method overestimates the fire resistance of the wall for R90 and R120.

7. CONCLUSIONS

An experimental and numerical analysis of the structural fire behaviour of a three-cell hollow concrete masonry wall was presented. The experimental program comprised four fire resistance tests and two loadbearing capacity tests after 90 minutes of fire exposure, in half-scale masonry walls. Different load levels were used and two repetitions were done for each load level. The experimental results were used to develop a FE model to predict the behaviour of these concrete masonry walls in fire, using the Abaqus Explicit software. The predictions of the model were compared with the experimental results in thermal and structural domain and a good agreement was reached. The numerical models allowed a detailed study on the behaviour of concrete masonry walls in fire situation.

The lack of material properties for masonry at high temperatures is an existing problem identified by many authors. The experimental characterization of masonry units and mortars under diversified load conditions at different temperature regimes, from ambient up to high temperatures would allow the development of more precise models. This data could then be used to feed the numerical models that can be further validated with experimental results of masonry walls at real scale.

The experimental and numerical results were compared to the tabulated data for fire design of masonry walls in terms of loadbearing capacity (**R**), insulation (**I**) and integrity (**E**). The loadbearing (**R**) criterion is related to the capacity of structural stability at high temperatures, the insulation criteria (**I**) is related to limiting the temperatures up to a certain value at the non-exposed face, and the integrity criterion (**E**) is related to preventing the fire spreading. It was found that the current values presented at the EN1996-1-2 are unsafe for the case of the masonry walls considered, overestimating the insulation capacity and the loadbearing capacity of these walls. The results were also compared with the simplified design method and it was found that this method overestimates the loadbearing capacity of the studied walls.

The following conclusions maybe drawn from this research:

- Concrete masonry is a heterogeneous material, as observed by the scatter on the temperatures, displacements and loads measured at the experimental tests for identical situations.

- Concrete masonry walls with dense aggregates and composed by group 2 masonry block units and with 100 mm in thickness are not able to fulfil the EI90, EI120 and EI180 requirements. Moreover, one of the studied walls was not able to fulfil the REI120 requirements for the load level α ≤ 1.0.

The load level α is defined by the ratio of the applied design load in the wall to its design resistance. Therefore, it seems that the values stated by tables N.B:3.1 and N.B.3.2 of EN 1996-1-2 [1] are unsafe for the analysed walls for both (**EI**) and (**REI**) fire resistance classes.

- The simplified calculation method presented in Annex C of EN 1996-1.2 [1] overestimates the fire resistance of this type of walls for R90 and R120.

- The proposed finite element model was capable to predict the behaviour of masonry walls composed by hollow concrete blocks from initial loading to the collapse in fire. The model was capable of predicting the initial thermal bowing and the subsequent reversal of the bowing phenomenon.

ACKNOWLEDGEMENTS

REFERENCES

[1] EN 1996-1-2 (2005), Eurocode 6 – Design of masonry structures, Part 1-2: General rules Structural Fire Design, European Committee for Standardisation, Brussels, Belgium.

[2] Dhanasekar M., Chandrasekaran V., Grubits S. J. (1994), A numerical model for thermal bowing of masonry walls. 10th IB2MaC, pp. 1093-1102.

[3] Nadjai A., O'Garra M., Ali F. A., Laverty D. (2003), A numerical model for the behaviour of masonry under elevated temperatures. Fire and Materials, 27-4, pp. 163-182

[4] Nadjai A., O'Garra M., Ali F. A., Laverty D. (2003), Finite element modelling of compartment masonry walls in fire. Computer and Structures 81, pp 1923–1930

[5] ISO 834-1 (1999), Fire resistance tests – elements of building construction, Part 1: general requirements. International Organization for Standardization, Geneva, Switzerland.

[6] EN1991-1-2 (2002), Actions on structures - Part 1-2: General actions - Actions on structures exposed to fire. European Committee for Standardization. Brussels, Belgium.

[7] Haach V. G. (2009), Development of a design method for reinforced masonry subjected to in-plane loading based on experimental and numerical analysis. PhD Thesis. University of Minho, Portugal.

[8] Byrne S. (1979), Fire resistance of load-bearing masonry walls. Fire Technology 15-3, pp 180-188.

[9] Lawrence S., Gnanakrishnan N. (1987), The Fire Resistance of Masonry Walls - An Overview. First National Structural Engineering Conference, Melbourne, Australia, pp 431-437

[10] Shields, TJ. O'Connor, DJ. Silcock, GWH. Donegan, HA. (1988), Thermal bowing of a model brickwork panel, Proceedings of 8th International Brick/Block Masonry Conference, Dublin, Vol. 2, pp. 846–856.

[11] Al Nahhas, F, Ami Saada R, Bonnet G, Delmotte P. (2007), Resistance to fire of walls constituted by hollow blocks: Experiments and thermal modelling. Applied Thermal Engineering 27-1, pp 258-267

[12] Nguyen T. D., Meftah F. (2012), Behaviour of clay hollow-brick masonry walls during fire. Part 1: Experimental analysis. Fire Safety Journal, 52, pp 55-64

[13] Andreini, M., Caciolai, M., La Mendola, S., Mazziotti, L., Sassu, M. (2015), Mechanical behaviour of masonry materials at high temperatures". Fire and Materials, 39, pp. 41–57.

[14] O'Meagher A. J., Bennetts I. D. (1991), Modelling of Concrete Walls in Fire. Fire Safety Journal, 17, pp 315-335

[15] Nguyen T.D., Meftah F. (2014), Behaviour of hollow clay brick masonry walls during fire. Part 2: 3D finite element modelling and spalling assessment. Fire Safety Journal, 66, pp. 35–45

[16] Kumar P., Kodur V.K.R. (2017), Modelling the behaviour of load bearing concrete walls under fire exposure. Construction and Building Materials, 154, pp. 993–1003

[17] EN 1996-1-1 (2005), Eurocode 6 – Design of masonry structures, Part 1-1: General rules for reinforced and unreinforced masonry structures, European Committee for Standardisation, Brussels, Belgium.

[18] EN 1052-1 (1999), Methods of test for masonry. Part 1 – Determination of compressive strength, European Committee for Standardisation, Brussels, Belgium.

[19] EN 1052-3 (2002), Methods of test for masonry: Part 3 – Determination of initial shear strength, European Committee for Standardisation, Brussels, Belgium.

[20] EN 1052-2 (1992), Methods of test for masonry: Part 2 – Determination of flexural strength, European Committee for Standardisation, Brussels, Belgium.

[21] EN 998-2 (2010). Specification for mortar for masonry – Part 2: Masonry mortar, European Committee for Standardisation, Brussels, Belgium.

[22] EN 1365-1 (2012), Fire resistance tests for loadbearing elements - Part 1: Walls, European Committee for Standardisation, Brussels, Belgium.

[23] Lopes R. (2017). Fire behaviour of structural masonry walls of vertical hollowed concrete blocks. MSc Thesis on Urban Fire Safety. University of Coimbra, Portugal.

[24] Lopes, R., Rodrigues, J. P. C., Pereira, J. M., Lourenço, P. B. (2017), Experimental research on structural concrete masonry walls subjected to fire, IFireSS 2017 – 2nd International Fire Safety Symposium, Naples, Italy.

[25] Lourenço P. B., Mendes N., Ramos L. F., Oliveira D. V. (2011) Analysis of masonry structures without box behaviour. Int. J Arch Heritage, 5:369–82

[26] Pereira J. M., Campos J., Lourenço P.B. (2015) Masonry infill walls under blast loading using confined underwater blast wave generators (WBWG). Engineering Structures, 92, pp. 69–83

[27] Abaqus User Manual (2010), Dassault Systems Simulia Corporation, USA.

[28] Zheng Y.; Taylor S. and Robinson D. (2010), Nonlinear finite element analysis of masonry arch bridges reinforced with FRP. ARCH'10 – 6th International Conference on Arch Bridges, pp 838-845

[29] Al-Gohi B. H., Demir C., Ilki A., Baluch M. H., Rahman M. K., Al-Gadhib A. H. (2012), Seismic vulnerability of multi-leaf heritage masonry walls using elasto-plastic damage model. In: Proc. of the international workshop: role of research infrastructure in seismic rehabilitation, Turkey.

[30] EN 1992-1-2 (2004), Eurocode 2 – Design of concrete structures, Part 1-2: General rules - Structural fire design, European Committee for Standardisation, Brussels, Belgium.

[31] Lubliner J., Oliver J., Oller S. and Onate E. (1989), A plastic-damage model for concrete. Int. J. Solids Struct.,25(3), pp 299–329.

[32] Lee J. and Fenves G. L. (1998), Plastic-damage model for cyclic loading of concrete structures. J. Eng. Mech. 124 (8), pp 892-900.

[33] EN 1363-1 (199), Fire resistance tests - Part 1: General requirements, European Committee for Standardisation, Brussels, Belgium.

[34] AS 3700 (2018), Masonry Structures, Standards Australia, Sydney, Australia.

TABLES

Table 1 – Masonry block units dimensions [7]

	X (mm)	Y (mm)	Z (mm)	a (mm)	b (mm)	Net area of blocks (cm²)	Area of voids (cm²)	Percentage of Voids (%)
Block	201	100	93	16	14	110.14	93.92	46
Half-Block	101	100	93	16	-	57.20	46.10	45

Table 2 – In-plane loads applied to the specimens [24]

Type of test	Specimen	Initial applied in-plane load (kN)	Initial In-plane load increasing rate (kN/s)	% f_{ak} EN 1052-1 [18]	% f_d EN 1996-1.1 [17]	In-plane load increasing rate after 90 min. of fire exposure (kN/s)
Fire resistance	1	208	0.5	30	70	---
	2					
	3	319	0.5	46	108	---
	4					
Loadbearing capacity at high temperatures	5	208	0.5	30	70	0.05
	6					

Table 3 – Experimental critical times

Specimen	Time of failure		E (min)	R (min)	Ultimate load (kN)	Maximum central displacement (mm)	Critical times (min)
	I (min)						
	At average temperature	At maximum temperature					
1	80	72	-	133	208	5.52	74
2	73	67	-	134	208	5.80	79
3	> 83	> 83	-	83	319	9.52	80
4	> 40	> 40	-	40	319	10.74	40
5	83	82	-	106	273	11.58	68
6	68	65	-	134	421	11.14	66

Table 4 – Comparison between experimental and numerical critical times

Specimen	Time of failure (Experimental tests)			Time of failure (Numerical simulations)		
	I (min)		R (min)	I (min)		R (min)
	At average temperature	At maximum temperature		At average temperature	At maximum temperature	
1	80	72	133	82	80	124
2	73	67	134	73	71	114
3	NA		83	NA		72
4	NA		40	NA		35
5	83	82	106	80	77	104
6	68	65	134	82	80	120

Table 5 – Tabulated data for fire resistance of masonry walls [1]

	Minimum wall thickness for fire resistance requirements						
	30 min	**45 min**	**60 min**	**90 min**	**120 min**	**180 min**	**240 min**
EI	50 mm	70 mm	70 to 100 mm	70 to 90 mm	90 to 200 mm	100 to 200 mm	125 to 200 mm
REI ($\alpha \leq 1.0$)	90 to 170 mm	100 to 170 mm	100 to 170 mm	100 to 170 mm	100 to 190 mm	140 to 240 mm	150 to 300 mm
REI ($\alpha \leq 0.6$)	90 to 140 mm	90 to 140 mm	100 to 140 mm	100 to 170 mm	100 to 170 mm	140 to 190 mm	150 to 240 mm

Table 6 – Fire resistance calculated based on the Eurocode's simplified calculation method

Time (min)	N_{rdfi} (kN)	Experimental results (kN)	Relative difference
30	558.2	> 319	-
60	385.4	> 208	-
90	344.9	273	-20.8 %
120	279.1	208	-25.5 %
180	204.0	-	-
240	152.5	-	-

FIGURES

      (a)   (b)   (c)
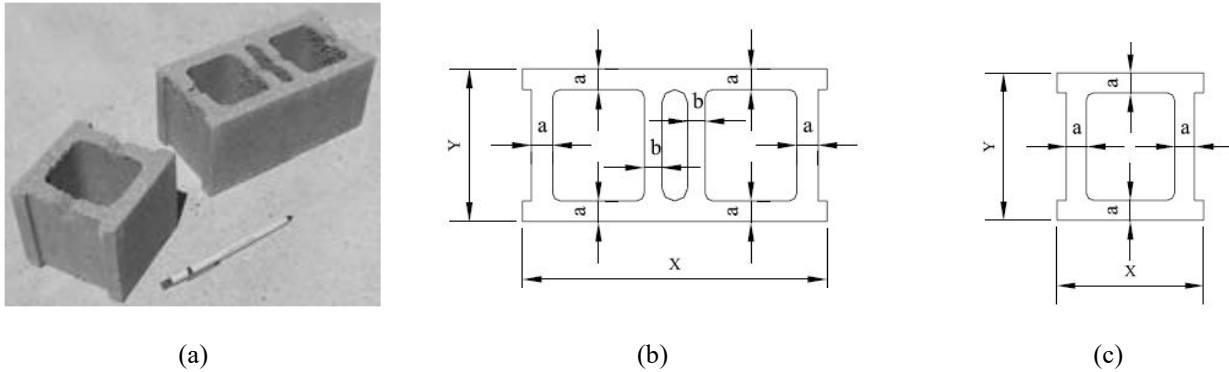
Figure 1 – Masonry units: (a) Half-scale block; (b) Block dimensions; (c) Half-block dimensions [7]

(a)   (b)
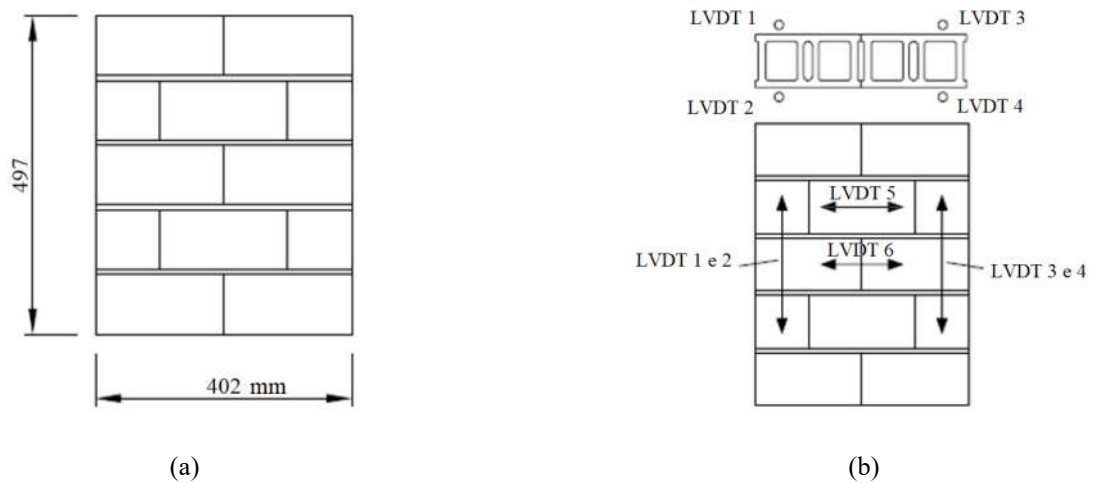
Figure 2 – Wall specimens: (a) Dimensions (in mm); (b) Instrumentation [7]

(a)   (b)   (c)
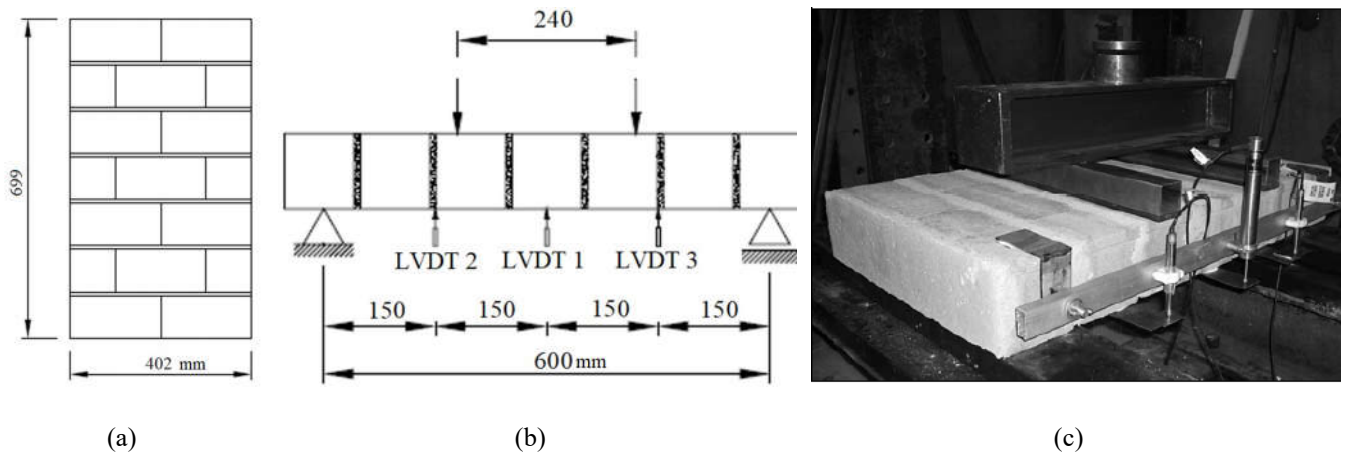
Figure 3 – Flexural tests: (a) Specimens dimensions; (b) Instrumentation; (c) Experimental setup [7]
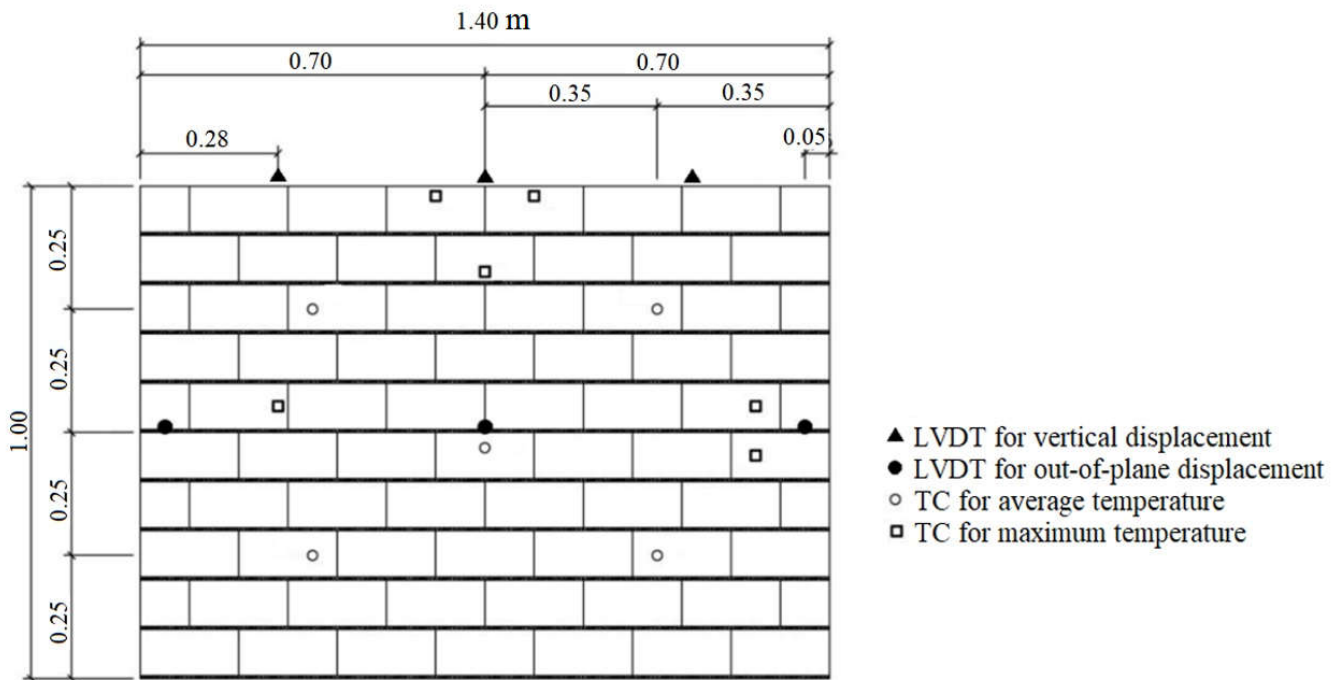
Figure 4 – Specimen dimensions and positioning of thermocouples and displacement transducers (dimensions in m) [24]

(a)   (b)
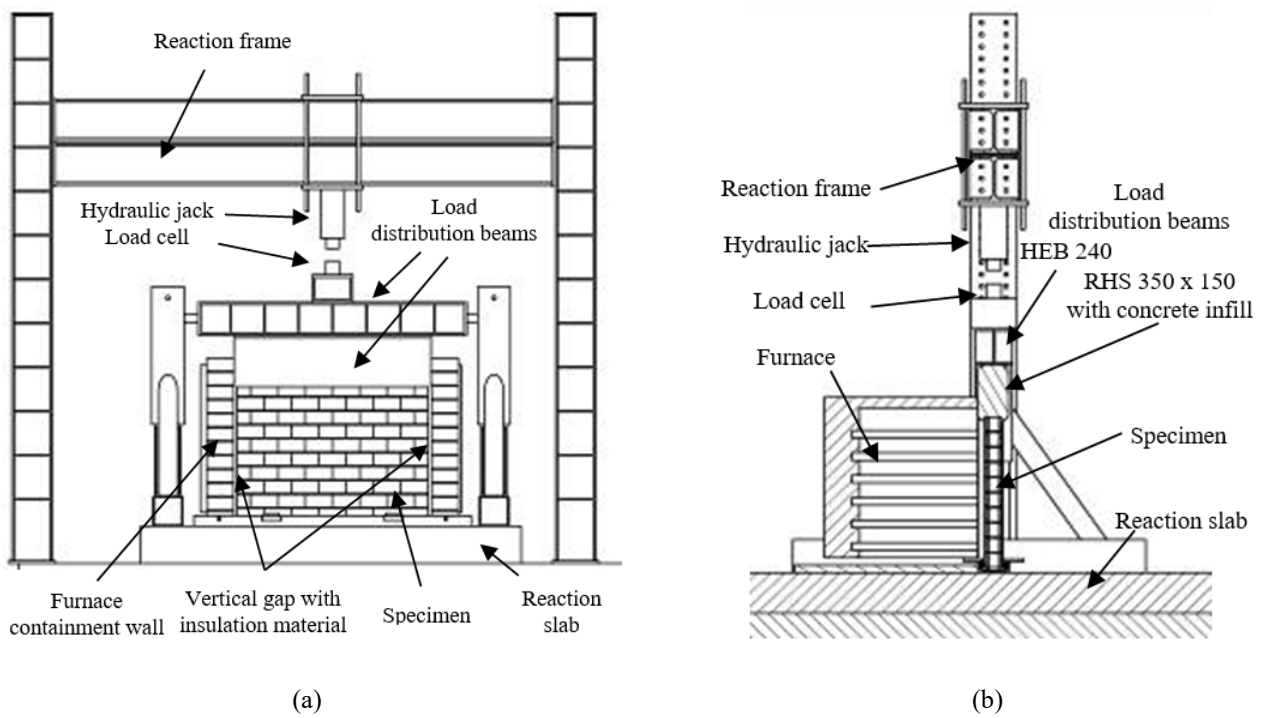
Figure 5 – Experimental setup: (a) Front view (b) Longitudinal view [24]

Figure 6 – Details of the experimental setup
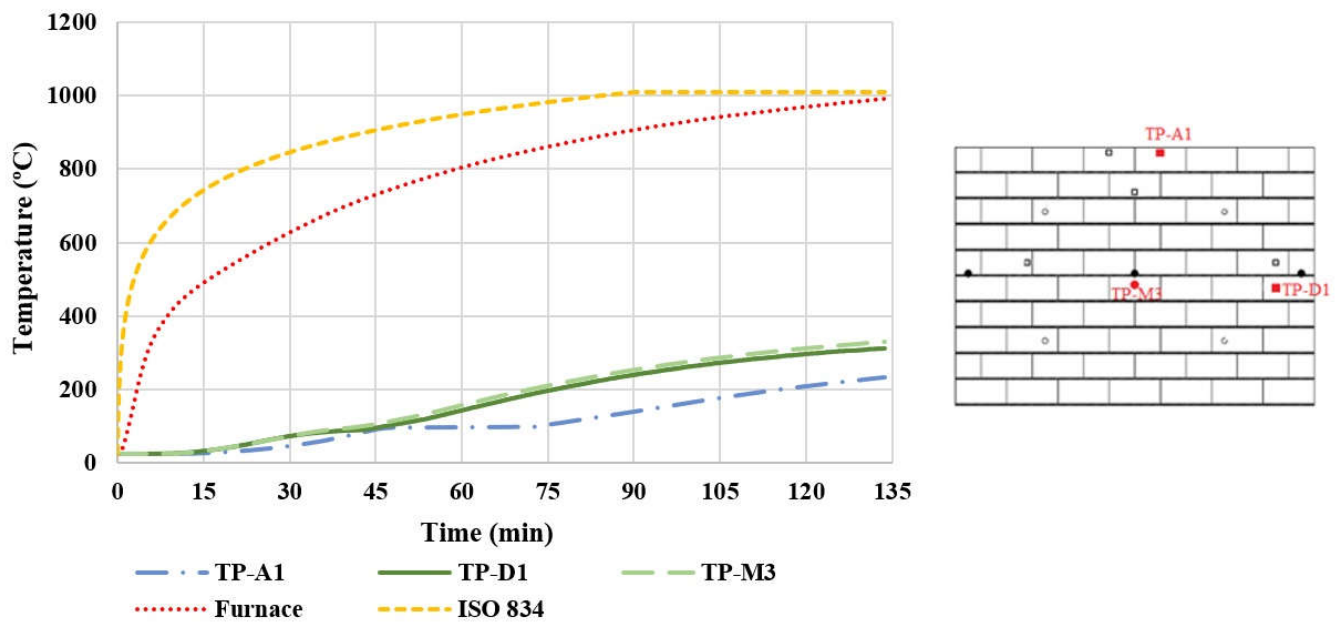
Figure 7 – Typical temperature evolution in specimen 6 as an example
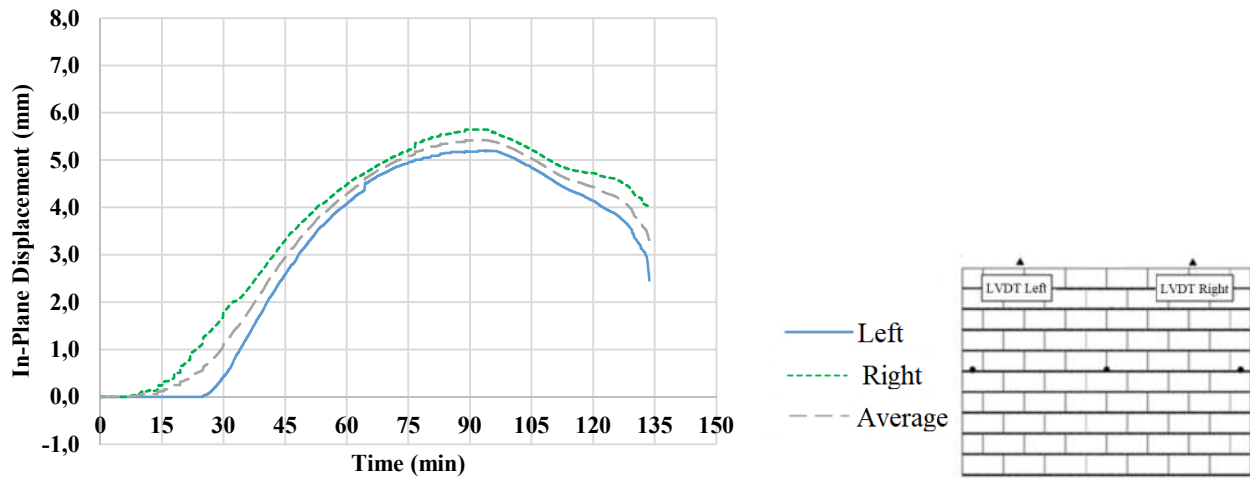
Figure 8 – In-plane displacements (Specimen 6)
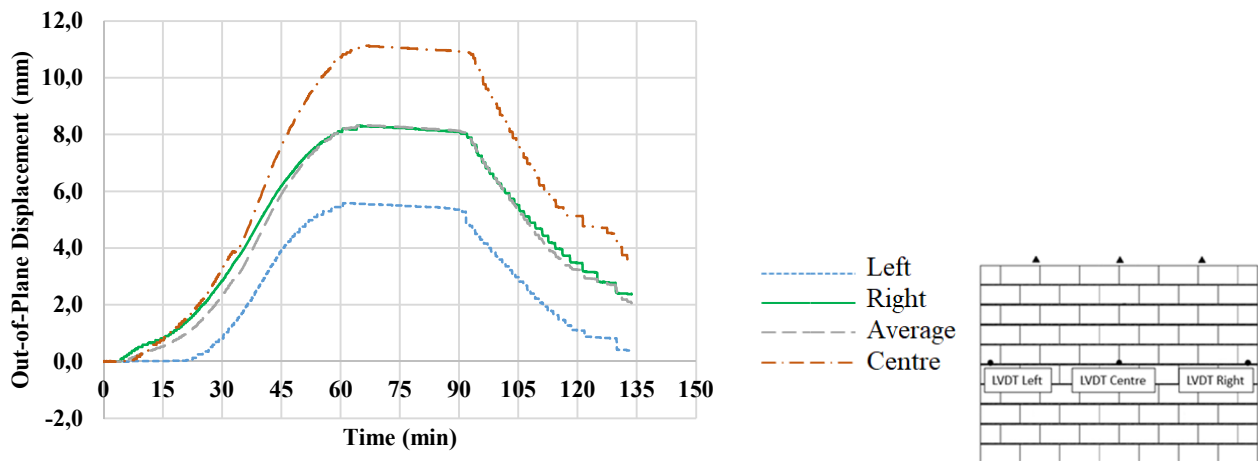
Figure 9 – Out-of-plane displacements (Specimen 6)

(a) Specimen 1   (b) Specimen 2

(c) Specimen 3   (d) Specimen 4

(e) Specimen 5   (f) Specimen 6
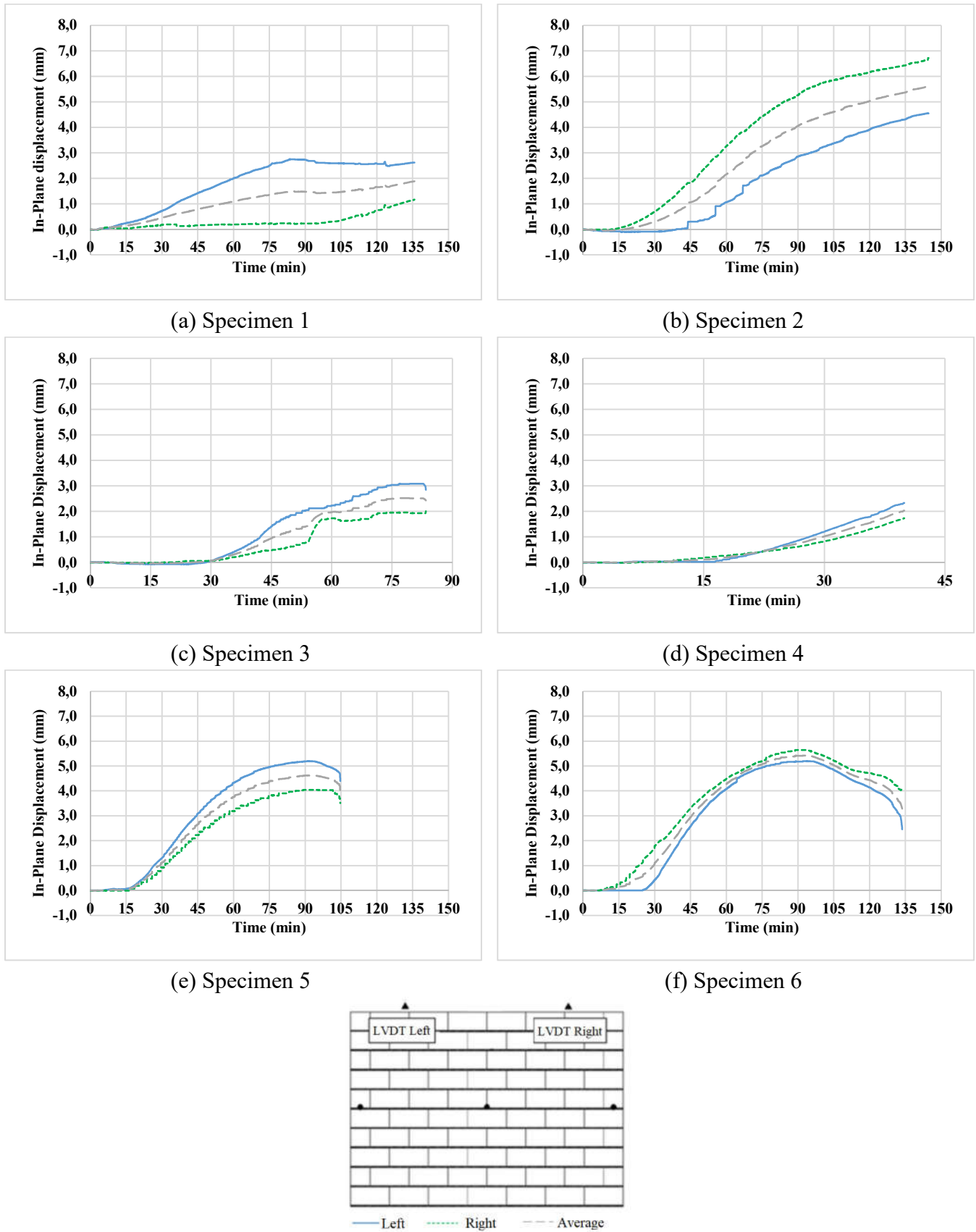
Figure 10 – Experimental results: In-plane displacement
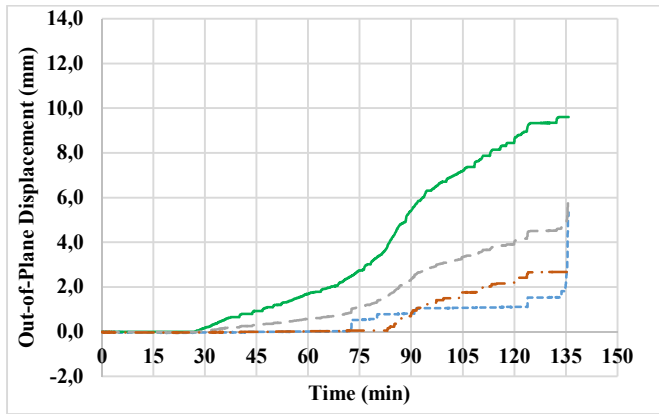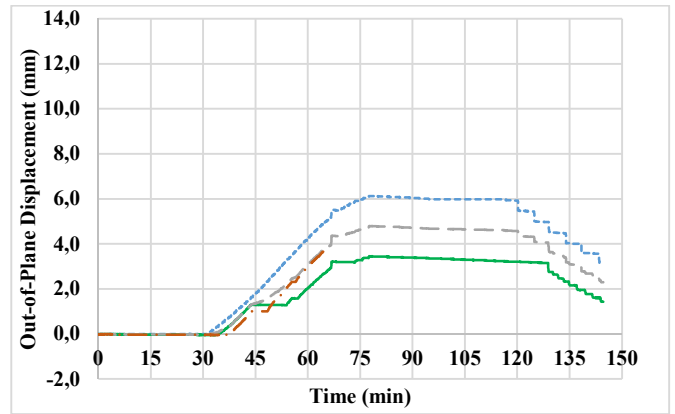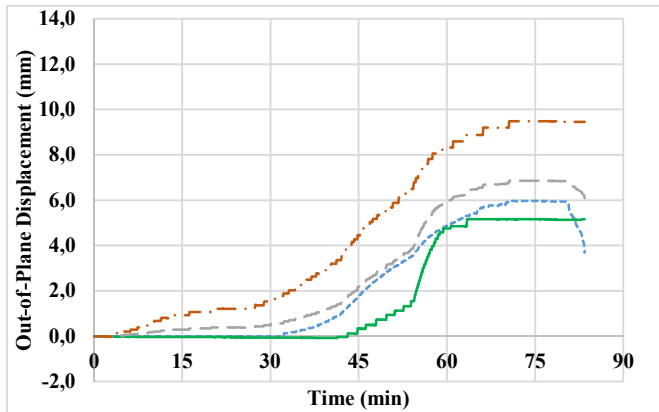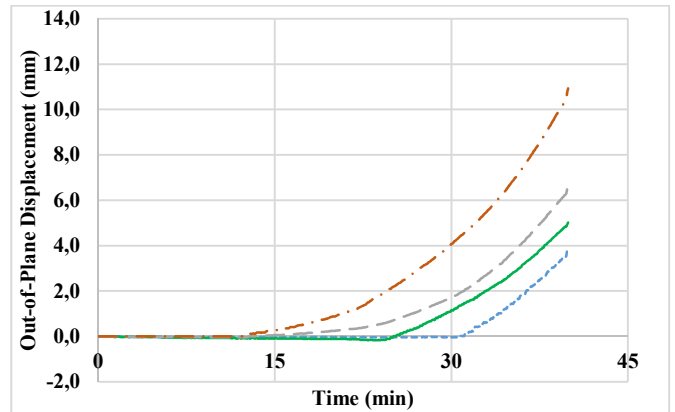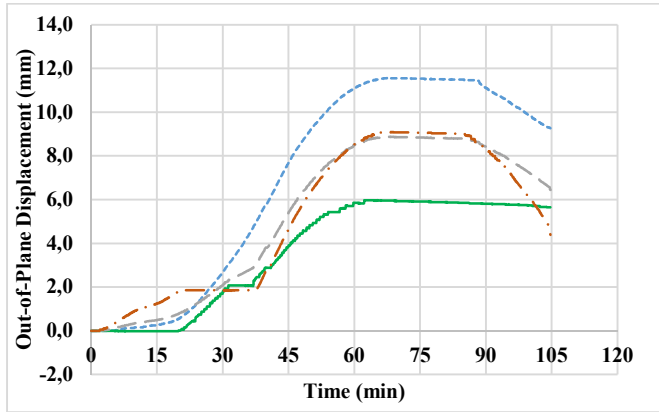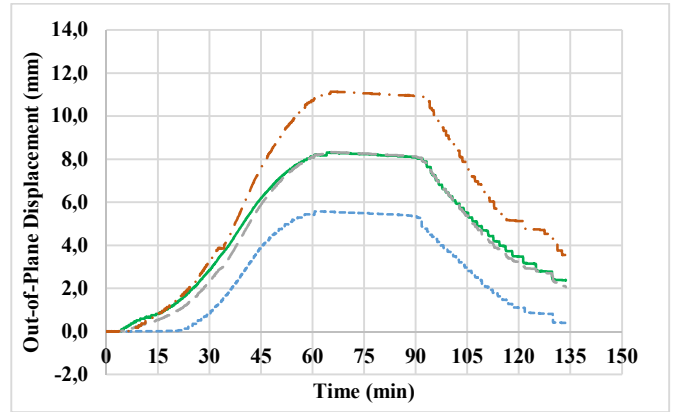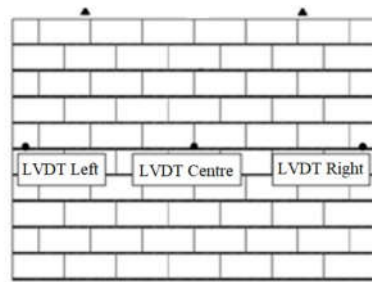
Figure 11 – Experimental results: Out-of-plane displacement

(a)　　　　　　　　　　　　　　　　(b)　　　　　　　　　　　　　　　　(c)

Figure 12 – Displacements evolution (Specimen 6): (a) Crack pattern on the unexposed face; (b) Spalling at the exposed face; (c) Vertical cracks at the middle of the wall

(a)

(b)

(c)

(d)
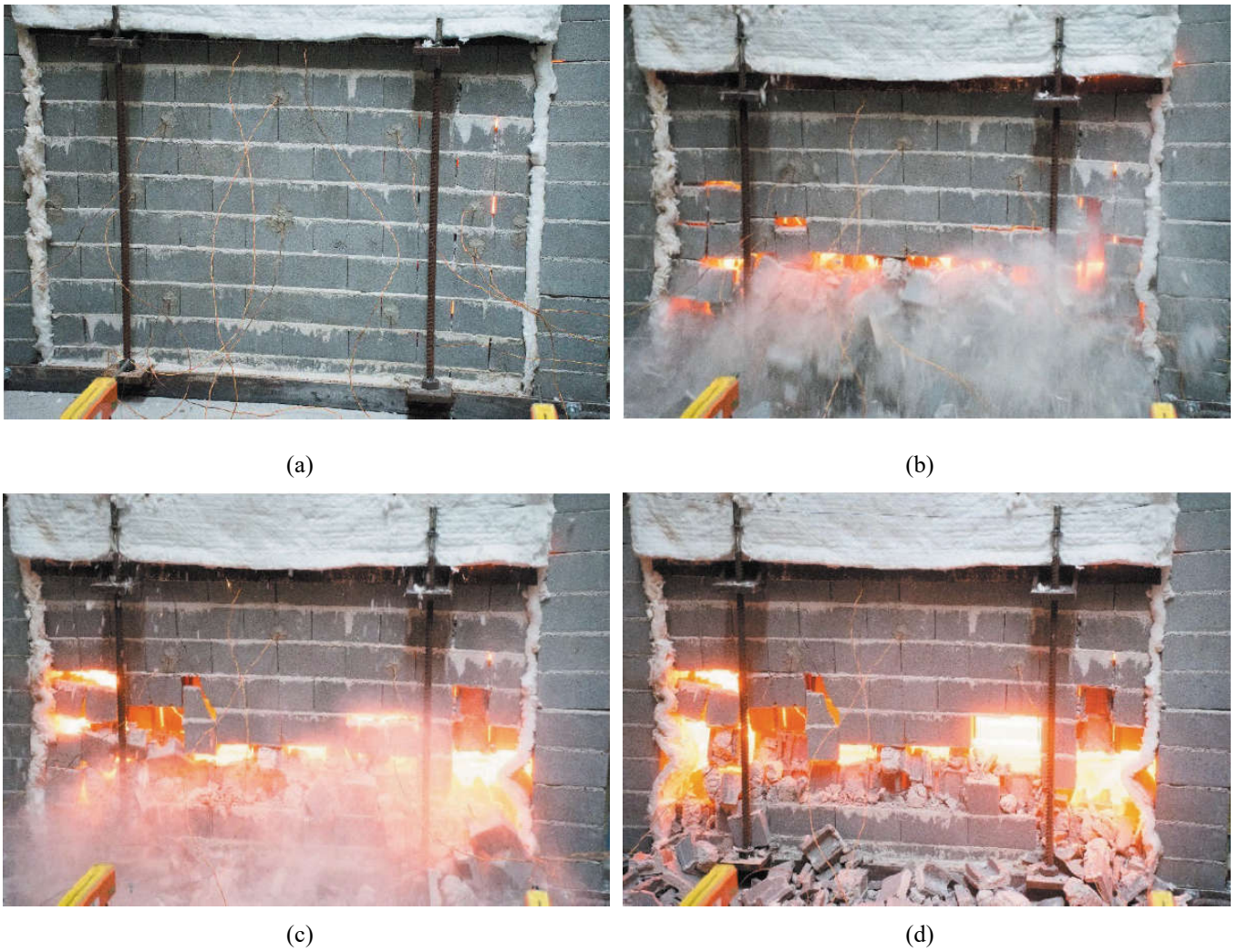
Figure 13 – Sequence of the sudden collapse (Specimen 6)
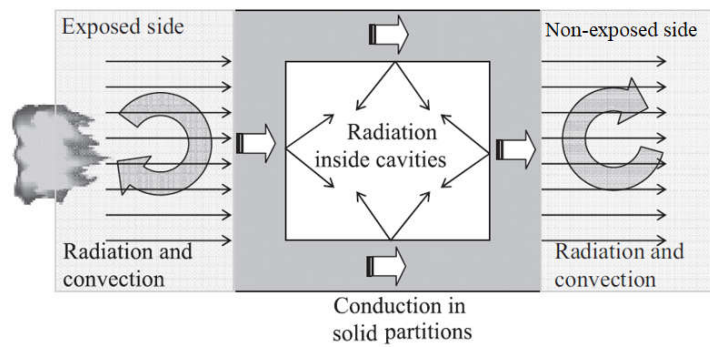
Figure 14 – Heat transfer process through a hollow block [15] (modified)
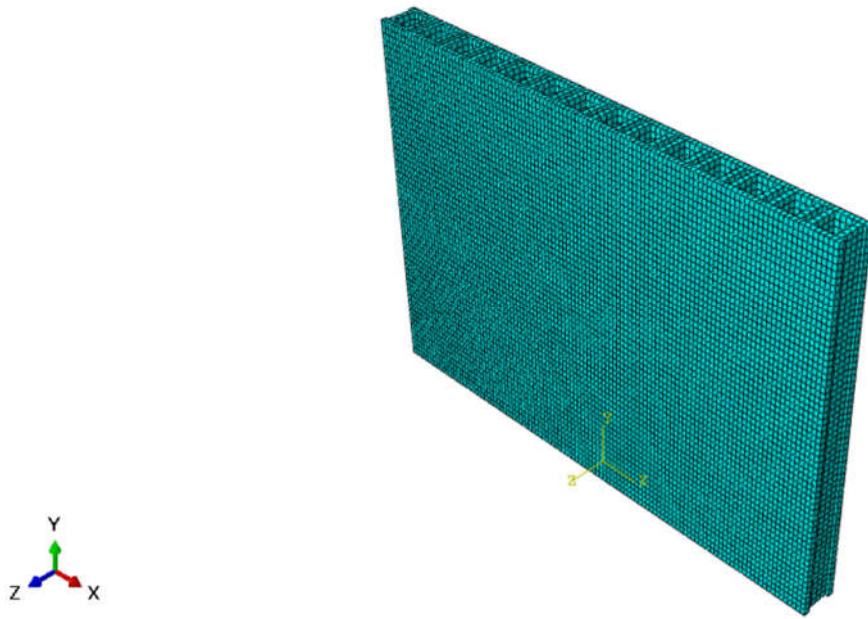
Figure 15 – Numerical model: mesh details
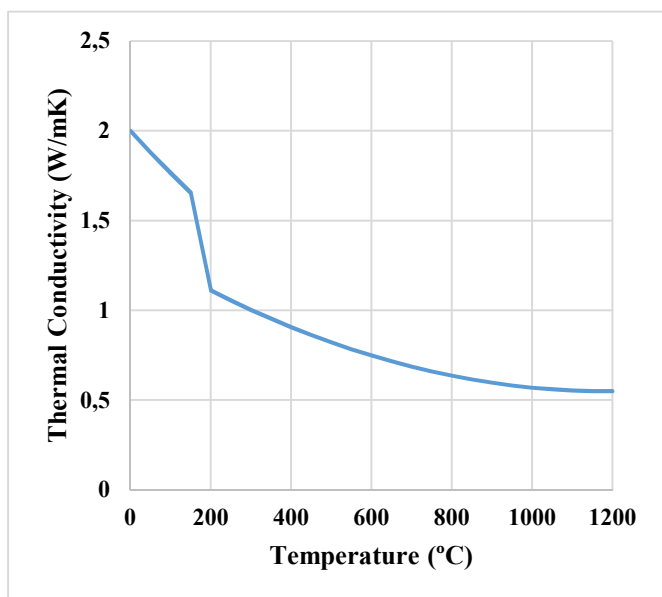
(a)
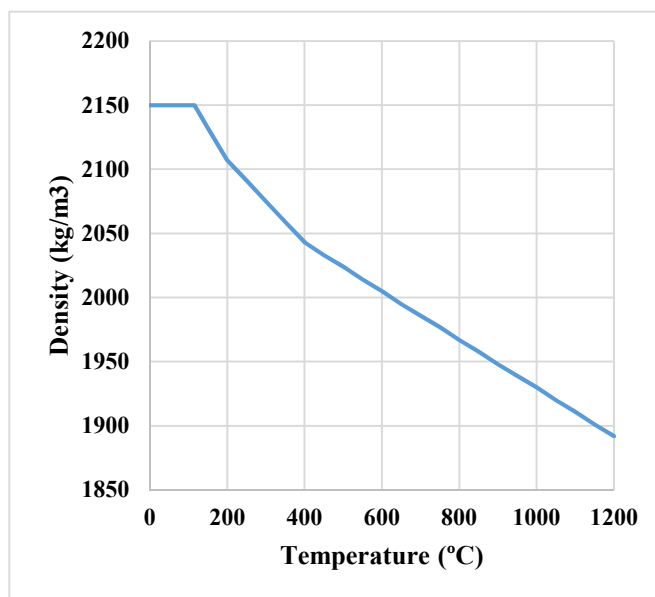
(b)
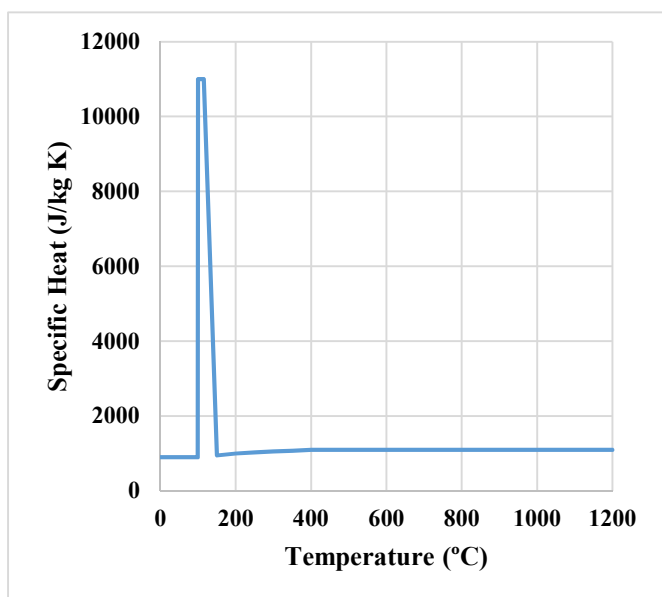
(c)
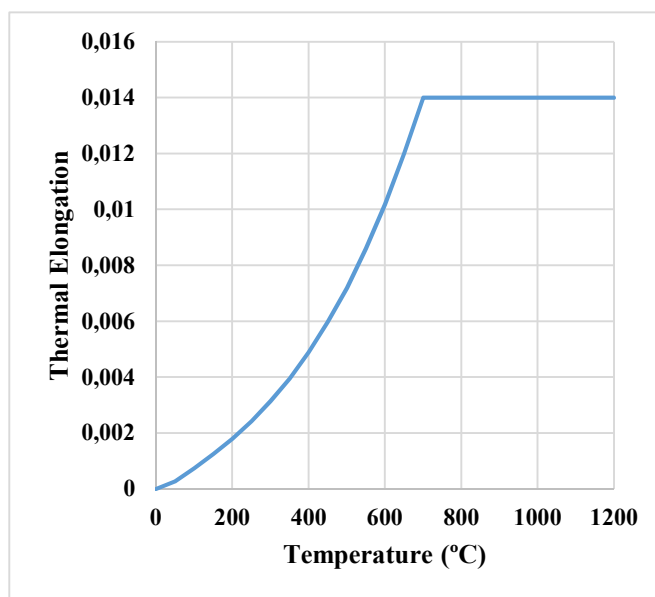
(d)

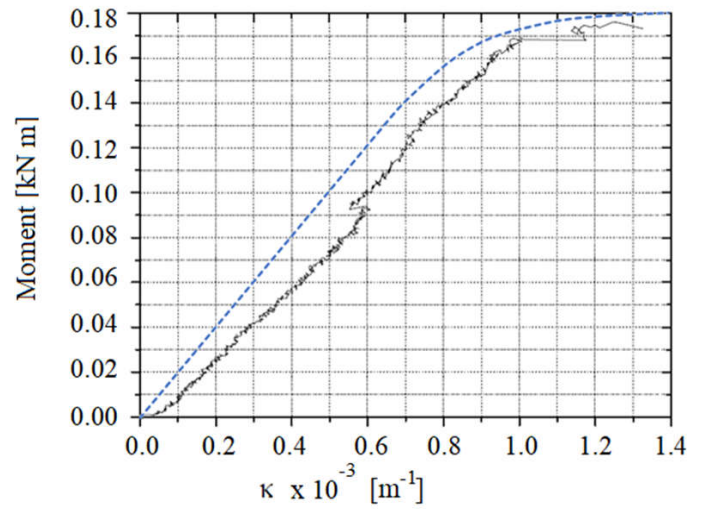**Figure 16 - Thermal properties: (a) Conductivity; (b) Density; (c) Specific heat; and (d) Thermal elongation**

(a) Specimen 1

(b) Specimen 2

(c) Specimen 3

(d) Specimen 4

(e) Specimen 5

(f) Specimen 6
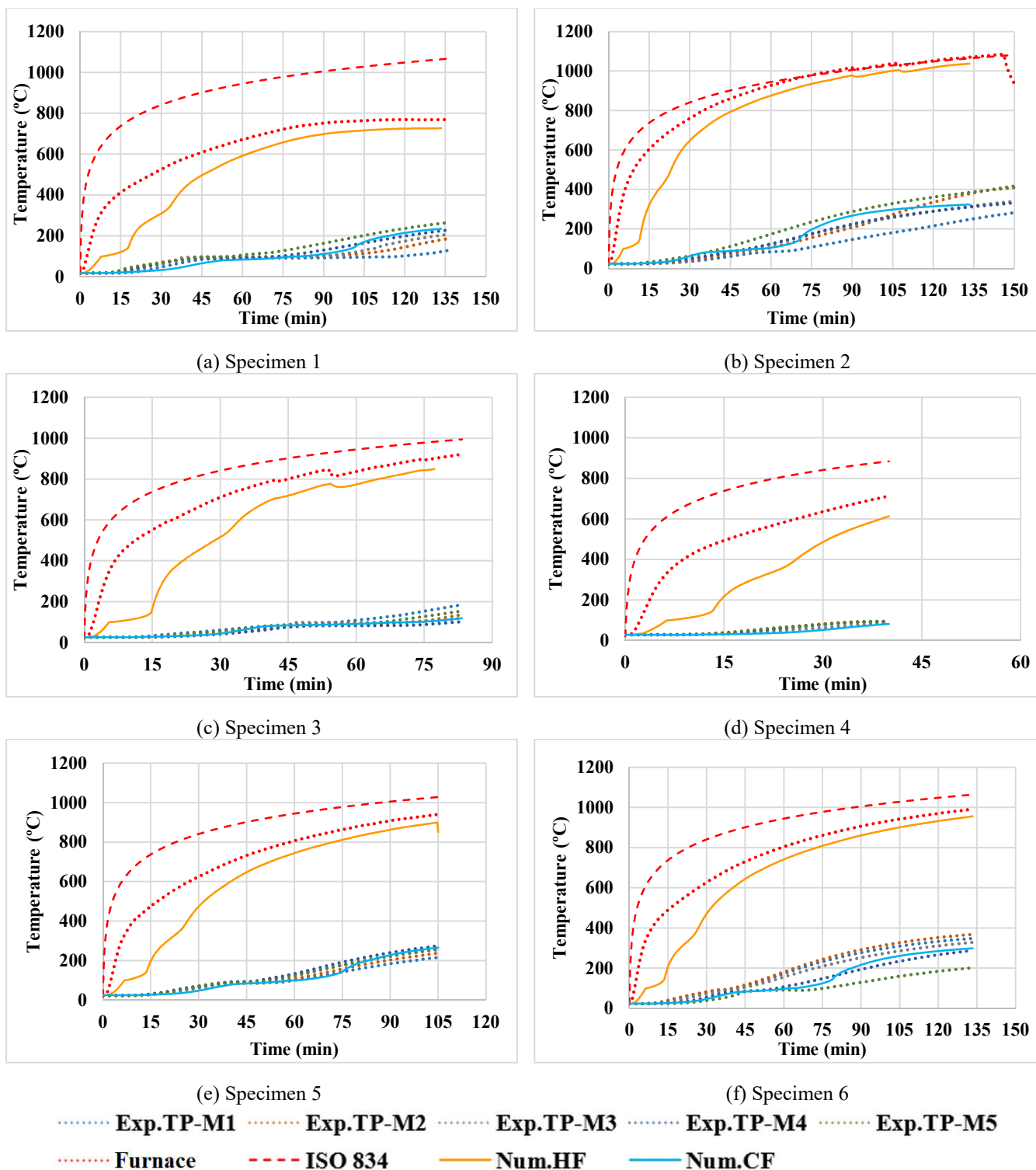
Figure 17 – Comparison of the FEA and experimental temperatures curves at the non-exposed face
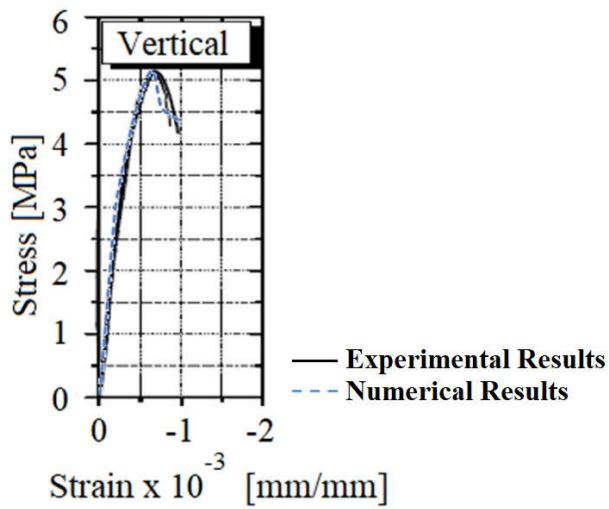
(a) Uniaxial compression normal to bed joints   (b) Four-point bending
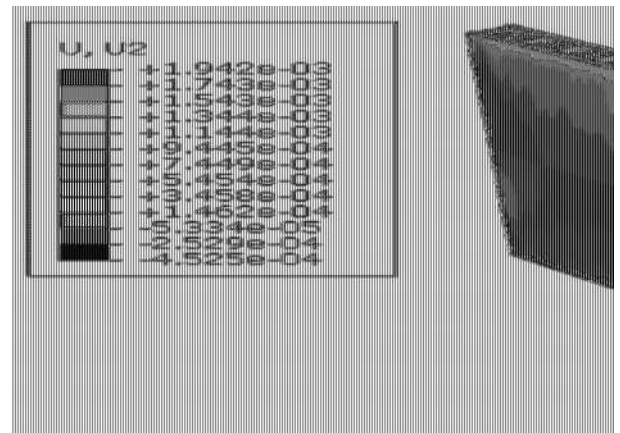
Figure 18 – Comparison of the FEA and experimental results at normal temperature
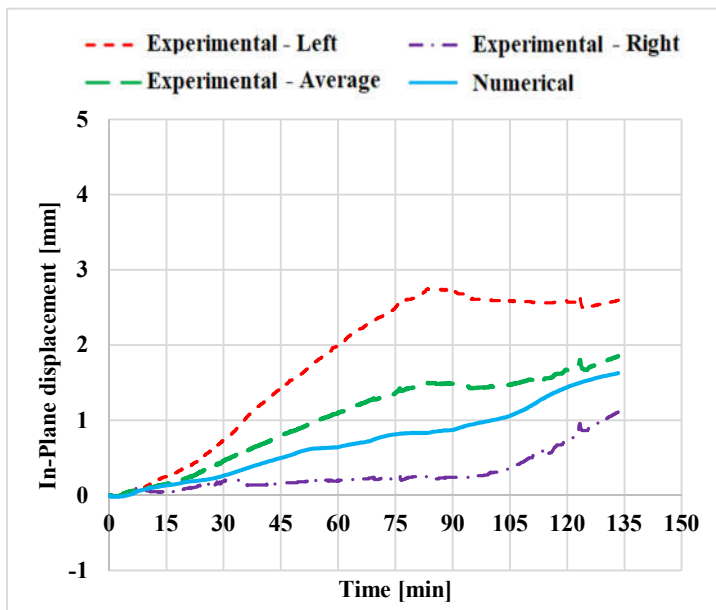
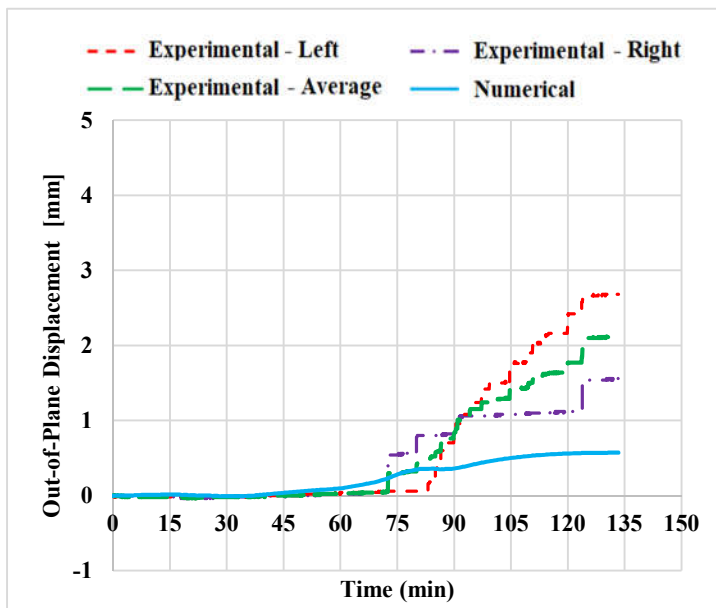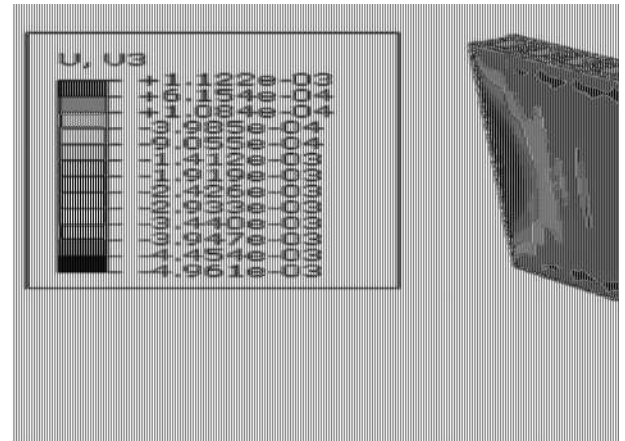(a)   (b)

Figure 19 – Specimen 1: (a) Comparison of the FEA and experimental vertical displacement; (b) vertical displacement fields at 130 min

(a)

(b)

Figure 20 – Specimen 1: (a) Comparison of the FEA and experimental out-of-plane displacement. (b) out-of-plane displacement fields at 130 min